Research Article | Vol. 29, No. 12 / 7 June 2021 / Optics Express 19126
Optics EXPRESS

Coherently-averaged dual comb spectrometer at 7.7 µm with master and follower quantum cascade lasers

K. KOMAGATA,[1,*] A. SHEHZAD,[1] G. TERRASANTA,[2] P. BROCHARD,[1] R. MATTHEY,[1] M. GIANELLA,[3] P. JOUY,[2] F. KAPSALIDIS,[4] M. SHAHMOHAMMADI,[4] M. BECK,[4] V. J. WITTWER,[1] J. FAIST,[4] L. EMMENEGGER,[3] T. SÜDMEYER,[1] A. HUGI,[2] AND S. SCHILT[1]

[1]*Laboratoire Temps-Fréquence, Institut de Physique, Université de Neuchâtel, Avenue de Bellevaux 51, 2000 Neuchâtel, Switzerland*
[2]*IRsweep AG, Laubisrütistrasse 44, 8712 Stäfa, Switzerland*
[3]*Empa, Laboratory for Air Pollution / Environmental Technology, 8600 Dübendorf, Switzerland*
[4]*Institute for Quantum Electronics, ETH Zurich, 8093 Zurich, Switzerland*
[*]*kenichi.komagata@unine.ch*

Abstract: We demonstrate coherent averaging of the multi-heterodyne beat signal between two quantum cascade laser frequency combs in a master-follower configuration. The two combs are mutually locked by acting on the drive current to control their relative offset frequency and by radio-frequency extraction and injection locking of their intermode beat signal to stabilize their mode spacing difference. By implementing an analog common-noise subtraction scheme, a reduction of the linewidth of all heterodyne beat notes by five orders of magnitude is achieved compared to the free-running lasers. We compare stabilization and post-processing corrections in terms of amplitude noise. While they give similar performances in terms of signal-to-noise ratio, real-time processing of the stabilized signal is less demanding in terms of computational power. Lastly, a proof-of-principle spectroscopic measurement was performed, showing the possibility to reduce the amount of data to be processed by three orders of magnitude, compared to the free-running system.

1. Introduction

In recent years, dual comb spectroscopy (DCS) has emerged as a new solution for fast and broadband spectroscopy [1]. Mid-infrared (MIR) quantum cascade laser (QCL) frequency combs [2] are an appealing and thriving technology for DCS [3,4], as they cover strong spectroscopic absorption bands of many relevant molecules in the MIR region. Dual QCL comb spectrometers have become commercially available as a table-top instrument, which is leading to new discoveries in many fields of science including biology and chemistry [5–12]. One key advantage of QCL-based DCS is the ability to perform studies with up to sub-microsecond time-resolution [11].

Moreover, QCL combs are very compact electrically-driven semiconductor light sources. Their longitudinal modes can be locked together through a four-wave mixing process [2] similar to the case of micro-resonator combs [13], leading to an equidistant comb spectrum, but which is not associated to the generation of soliton pulses in contrast to micro-resonators. QCLs do not require optical pumping, in contrast to other optical frequency comb (OFC) sources, which are based on optically-pumped gain [14] or nonlinear materials [15]. Thus, the comb properties can be directly controlled through the laser driving current, the chip temperature [3] or by radio-frequency (RF) injection of the repetition frequency [16–18]. These are key advantages for system integration.

#425480 https://doi.org/10.1364/OE.425480
Journal © 2021 Received 7 Apr 2021; revised 12 May 2021; accepted 18 May 2021; published 4 Jun 2021

Optics EXPRESS

Furthermore, the control with the laser driving current and by RF injection is fast, enabling high locking bandwidths to be achieved or the possibility of fast frequency scanning of the comb spectrum [4].

In state-of-the-art DCS with MIR QCL combs, the multi-heterodyne beat signal is typically composed of 100 to 250 lines and spans an RF bandwidth of 400 MHz to 900 MHz [3,4,8,19,20]. The linewidth of the optical modes in free-running operation is in the megahertz range, which is largely sufficient to resolve relevant spectroscopic features in many applications [4,8,11]. The interferogram is then typically digitized with 12-bit to 16-bit resolution at 1.6 GS/s to 2.5 GS/s [3,4,11]. The reported implementations use two detectors for the sample and reference signals, respectively, such that the size of the data to be processed is between 4.8 GB/s and 8 GB/s. As a comparison, with fiber mode-locked lasers in the near-infrared (NIR), the data rate is on the order of 400 MB/s [1] with typically more than 100'000 lines comprised in an RF bandwidth of 50 MHz [21]. We note that NIR fiber mode-locked lasers typically have repetition rates of a few hundred MHz compared to multiple GHz for QCL combs.

The large data rate encountered with QCL DCS is cumbersome for storage and processing, and may lead to low measurement duty cycles. A solution to this issue that is widely used with NIR systems is real-time coherent averaging. Coherent averaging is a processing method used to isolate the periodic components of a signal [22], which can reduce the amount of data to handle in some conditions. Coherent averaging of the digitized signal can be implemented with different (and potentially combined) approaches: full or relative locking of the two combs [23–29], correction of the noise of the multi-heterodyne signal using various types of error signals [21,23,24,30–32], or computational processing without requiring additional information on the system other than the interferogram [33–36]. The last approach has been used with MIR QCL frequency combs, but remains challenging to implement in real-time due to the large data rate, even if recent works have shown that it is possible using adequate hardware and parallel processing on graphics processing unit (GPU) [37].

Regarding the two other approaches that are routinely used with NIR lasers (i.e., full or relative locking of the two combs, correction using error signals), the known solutions cannot be implemented in a straightforward manner with MIR QCL-based DCS because of the lack or poorer availability of required optical components in the MIR. Moreover, the specificity of QCLs is also an opportunity to implement other techniques to achieve a mutual lock between the two combs, such as RF injection locking. Although the mutual lock of one degree of freedom between two QCL combs has been reported [38], it has not been the case so far for a full mutual lock to the best of our knowledge. One further interest to apply a mutual lock is that it represents an intermediate step towards a full independent stabilization of the two combs, which is highly desirable in a high-resolution spectrometer [4].

In this work, we mutually locked a pair of QCL combs in their two degrees of freedom in a master-follower scheme (also known as master-slave scheme). To further reduce the relative offset-frequency fluctuations, a common-mode noise subtraction (CMNS) scheme was implemented as an alternative approach from Refs. [21,39]. This allowed us to perform coherent averaging of the spectroscopic signal, and to compare those performances with post-processing corrections using the signal from the reference photodiode.

The outline of the paper is as follows: The experimental setup with the implemented relative frequency stabilization and noise compensation scheme is described in Section 2. The performance of the system in terms of frequency stability is reported in Section 3 and a proof-of-principle spectroscopic demonstration with coherent averaging is presented in Section 4. Finally, Section 5 presents the conclusion and outlook of this work.

Optics EXPRESS

2. Experimental setup

In this section, we describe the experimental setup of our DCS system. Notably, we implemented a mutual lock of two QCL combs. We used an all-RF scheme to further lower the phase fluctuations of the interferogram and remove its offset frequency in order to fulfill the conditions necessary for coherent averaging, which is to have a harmonic comb in which the frequency of each comb line is an exact multiple of their spacing.

2.1. Dual QCL comb system

The experimental setup implemented for dual-QCL-comb spectroscopy and frequency stabilization of the multi-heterodyne signal is schematized in Fig. 1. Two mid-infrared QCL combs emitting in the 8-µm spectral range are heterodyned on two fast photodiodes (Vigo models PV-3TE-10.6-0.05 × 0.05 and PV-4TE-10.6-0.1 × 0.1 with 1-GHz bandwidth) for sample and reference measurements. The sample is placed in one of the combined beam paths for absorption DCS, whereas the signal from the second detector is used for normalization.

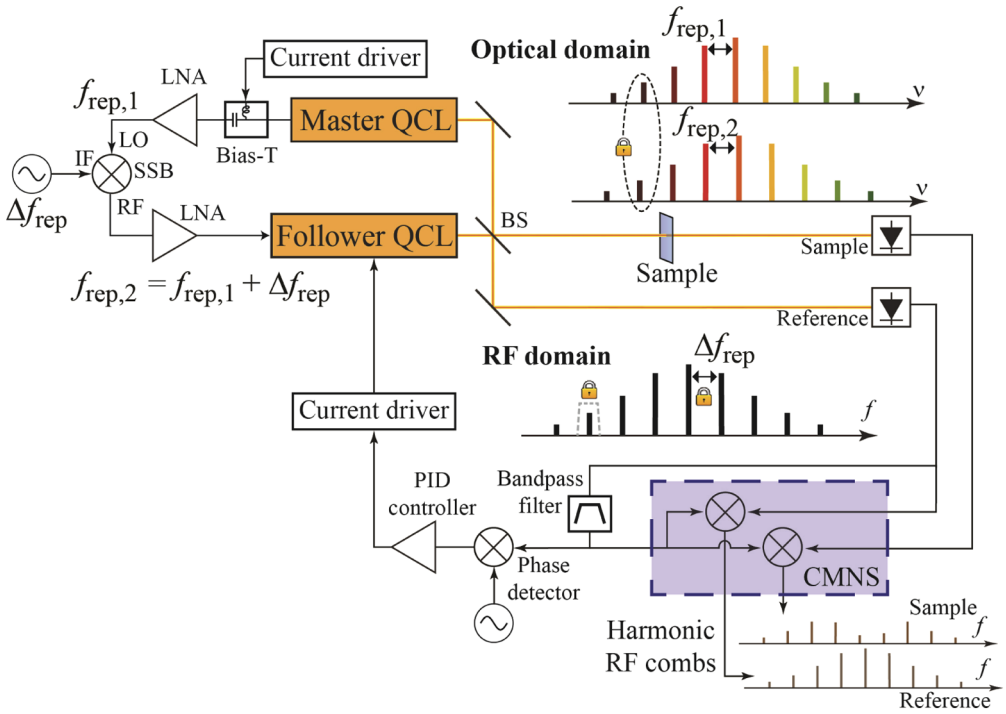

Fig. 1. DCS setup and master-follower stabilization. Two QCL combs are heterodyned on two photodiodes (reference and measurement channels), leading to RF combs in the photodiode output signals. The injection of the frequency-shifted intermode beat frequency from the master to the follower QCL locks the mode spacing of the RF comb. In addition, an optical line of the follower QCL comb is locked to one line of the master QCL comb by stabilizing the frequency of their heterodyne beat. The beat frequency is compared in phase to a reference oscillator and a correction signal is fed back to the follower QCL as a modulation of the driving current. The common-mode noise subtraction scheme (CMNS) is schematized in the dashed box and is described in detail in the Appendix. LNA: low noise amplifier, SSB: single sideband mixer.

The first QCL acts as a master comb. It is operated at a temperature of 23°C and is driven at an average current of ~1420 mA. The resulting comb spectrum centered around 1275 cm^{-1} spans

Optics EXPRESS

over about 40 cm^{-1}. The spacing between the comb modes is $f_{rep,1}$ = 9.70 GHz. The beating of the modes in the laser cavity modulates the current in the QCL and produces a so-called intermode beat signal at $f_{rep,1}$ [40]. A bias-tee is used to enable simultaneous direct current drive of the QCL and RF extraction of the electrical intermode beat signal. The extracted signal has a power of roughly −80 dBm. The second QCL acts as a follower laser that is phase-locked to the master to achieve their relative stabilization (see Section 2.2). It is operated at ~1050 mA and 24°C and emits a comb spectrum spanning from 1290 cm^{-1} to 1300 cm^{-1}. Its mode spacing is typically 45 MHz higher than for the master QCL. The operation points of the two QCLs are slightly varied depending on the time of the measurement to ensure a low-noise comb operation for each of them (characterized by a narrow intermode beat signal < 10 kHz), as the same operating point did not always result in the same comb state. The comb state is also chosen to limit the bandwidth of the generated multi-heterodyne beat signal, shown in Fig. 2, to less than 1 GHz with approximately 15 comb lines (11 lines in a 25-dB bandwidth). The incident power on the photodiodes is attenuated to approximately 1 mW with neutral density filters and wire grid polarizers. The follower QCL is mounted in a dedicated package with an RF port connected to the laser that is distinct from the driving current port and is optimized for efficient RF extraction/injection. Injecting an RF signal with a frequency that is close to the native mode spacing of the QCL can force it to operate at the injected frequency (RF injection locking), therefore locking its mode spacing [2,16–18].

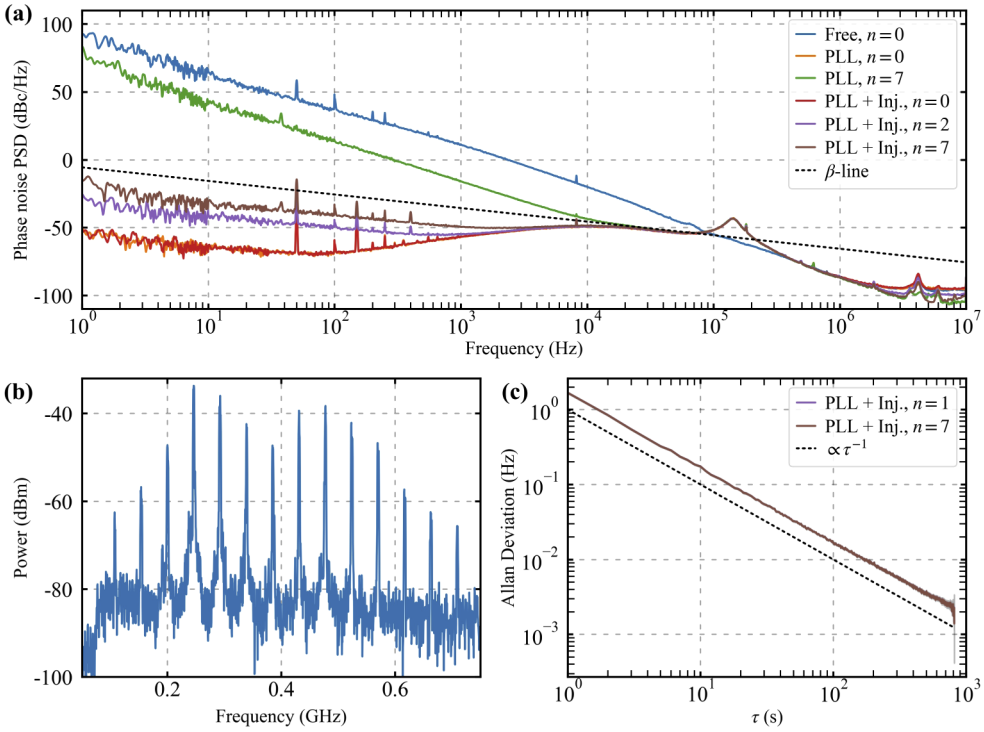

Fig. 2. Evaluation of the master-follower stabilization. (a) Phase noise PSD of different lines of the RF comb in the free-running case (Free), with the PLL activated (PLL) or with both PLL and RF injection locking (PLL + Inj.). The orange line (PLL only for $n = 0$) is almost exactly hidden by the red line (PLL + Inj. for $n = 0$). (b) Typical spectrum of the multi-heterodyne beat. The exact shape may vary. (c) Allan deviation of the frequency of two different lines that show a high overlap.

Optics EXPRESS

2.2. Master-follower QCL stabilization

RF injection is used to lock one degree of freedom of the follower QCL to the master QCL. This is achieved by extracting the intermode beat signal from the master QCL using a bias-tee. The extracted signal is then amplified, up-shifted by approximately 45 MHz using a single sideband (SSB) mixer and injected in the follower QCL after further amplification to ~5 dBm. To achieve a full relative phase lock of the follower QCL to the master QCL, its second degree of freedom is stabilized by phase-locking one line of the multi-heterodyne beat signal to a reference RF oscillator. A comb line at ~200 MHz in the reference RF comb is filtered with a narrowband filter and compared in phase to a reference oscillator in a digital phase detector (DXD200 from Menlo Systems). The resulting phase error signal is amplified in a proportional-integral-derivative (PID) servo-controller (Vescent D2-125) and corrects the follower QCL by feedback to the driving current. All electronic oscillators used in the locking scheme are referenced to a hydrogen maser to ensure their long-term stability.

2.3. Common mode noise subtraction scheme

An analog CMNS scheme is used to remove the offset frequency of the RF combs and the remaining common frequency noise among their lines [21,39]. Removing the offset frequency is necessary for coherent averaging [24]. The principle is to isolate one spectral line of the multi-heterodyne signal and to mix it with the entire RF comb to produce their frequency difference. The resulting RF comb is offset-free, i.e., it constitutes a harmonic comb, in which the common noise between all lines has been furthermore removed. We implemented a different CMNS scheme than reported in Refs. [21,39], which is described in the Appendix. We note that unlike Ref. [21], this scheme does not require additional optical components, which is possible as the RF comb modes are well resolved.

3. Evaluation of the stabilization schemes

3.1. Master-follower stabilization

The master-follower scheme described in Fig. 1 was implemented by first stabilizing one line of the RF comb at 200 MHz to a reference signal using a phase-lock loop (PLL). The phase noise of different lines of the reference RF comb was measured using a phase noise analyzer (Rohde & Schwarz FSWP-26) and is displayed in Fig. 2(a). The line $n = 0$ at 200 MHz used for the phase-lock shows a noise reduction of 140 dBc/Hz at 1-Hz Fourier frequency as a result of the stabilization. The locking bandwidth is 100 kHz, assessed from the servo bump in the noise spectrum. Other lines, e.g., $n = 7$ (the 7^{th} line from the locked line) showed only ~15 dBc/Hz noise reduction when solely the PLL was activated. The remaining noise likely results from the relative frequency fluctuations between the mode spacing of the two QCL combs.

In a second step, we added a relative stabilization between the mode spacing of the two QCL combs by RF extraction/injection as described in Section 2.2. The locking range was in the order of 200 kHz, enabling small tuning of Δf_{rep}. The RF injection sometimes led to a state change of the follower comb. We believe that the injection of the RF power heats the laser, which can cause a change of state.

With the combined RF injection locking of the mode spacing of the follower QCL and phase-lock of the RF comb line at 200 MHz, the other lines of the multi-heterodyne spectrum showed a large phase noise reduction compared to the case of the PLL only [see Fig. 2(a)]. We used the β-separation line approximation [41] to estimate the linewidth of the RF comb modes from their corresponding phase noise power spectral density (PSD). The free-running linewidth of 1 MHz (at 1-s integration time) calculated for the line $n = 0$ is reduced to 700 kHz with the master-follower stabilization scheme. This marginal linewidth reduction relative to the large decrease observed for the phase noise PSD results from the phase noise bump added by the

Optics EXPRESS

PLL, which has a large impact on the linewidth as it occurs at high Fourier frequencies (~100 kHz) [42].

Even with RF injection-locking of the mode spacing, the phase noise of the RF comb modes at Fourier frequencies between 1 Hz and 1 kHz increases with the mode index. We infer that that it is due to the residual noise of the mode spacing difference Δf_{rep} between the two QCL combs. Neglecting the correlations between the frequency fluctuations of Δf_{rep} and of the locked line frequency f_0, the frequency noise (FN) PSD of Δf_{rep} can be estimated as $S_{f_{\mathrm{rep}}} = (S_0 - S_n)/n^2$, where S_0 and S_n are the FN-PSD of the locked line f_0, and of the analyzed line of index n, respectively. The results are consistent when computed from lines 1, 3, and 6 [data from Fig. 3(a)], leading to an FN-PSD of Δf_{rep} of $5.3 \cdot 10^{-4}$ Hz^2/Hz at 1-Hz Fourier frequency.

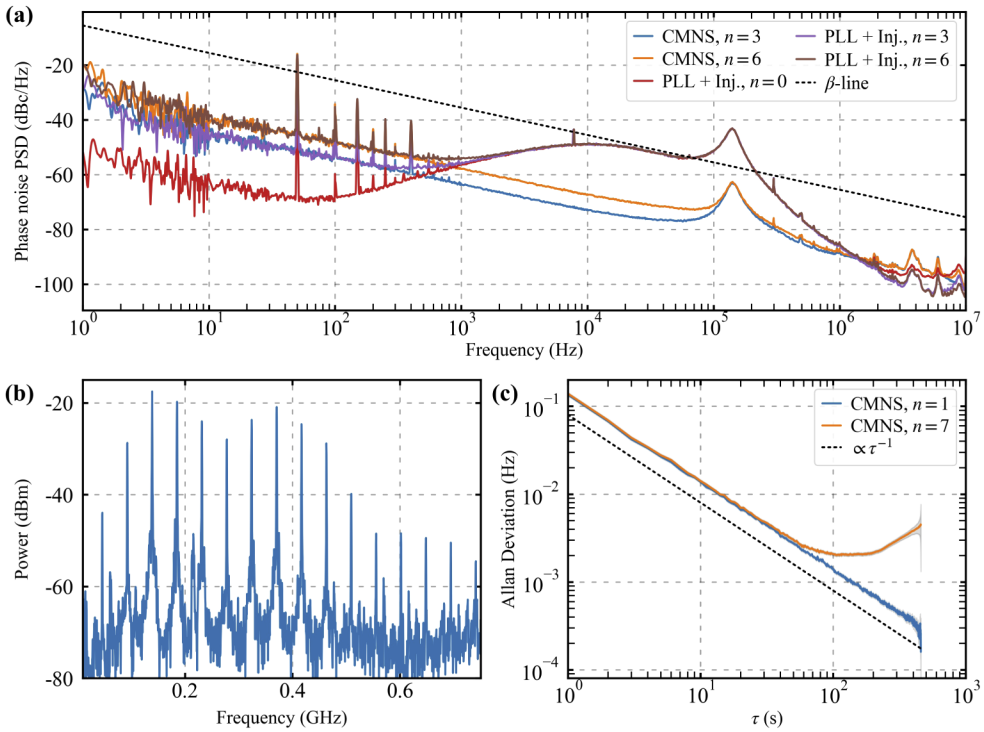

Fig. 3. Evaluation of the CMNS. (a) Phase noise PSD of different lines of the RF comb in the master-follower configuration with CMNS and without (PLL + Inj.). (b) Typical spectrum of the multi-heterodyne beat. The exact shape may vary. (c) Allan deviation of two different lines of the RF comb.

The long-term frequency stability of the fully-stabilized RF comb was investigated by measuring the frequency of different lines using a multi-channel Π-type frequency counter (FXM-50 from Menlo Systems). Lines $n = 1$ and $n = 7$ were frequency down-converted to < 50 MHz within the counter bandwidth so that they can be simultaneously measured. Allan deviations calculated from the recorded time series of these lines show Hz-level fluctuations at 1-s averaging time, averaging down to below 10 mHz at integration times longer than 200 s [see Fig. 2(c)].

3.2. Common-mode noise subtraction

The phase noise of the RF comb lines was further lowered using the CMNS scheme in addition to the mutual stabilization. The frequency fluctuations of the phase-locked RF comb line at ~200 MHz were subtracted from the entire comb spectrum as described in Section 2.3.

Optics EXPRESS

The noise-compensated spectrum displayed in Fig. 3(b) has the same overall envelope as the original one within 3 dB. This does not compromise spectroscopic measurements to be achieved, even if the sample and reference measurements can be affected slightly differently, as a time-sequential calibration scheme is usually used in QCL DCS (sample and background spectra successively measured) [4]. Furthermore, the reference channel is mainly used for amplitude noise compensation by normalization. Some spurious weaker lines appear between the main comb lines in the common-noise-compensated spectrum, resulting from different mixing products that may occur in the noise compensation scheme. These spurious lines are not problematic as their contribution to the processed spectrum is made negligible by the coherent averaging process.

The phase noise measured for lines $n = 3$ and $n = 6$ of the noise-compensated spectrum is displayed in Fig. 3(a). These lines correspond to components at 342 MHz and 485 MHz of the initial RF comb and are shifted to 142 MHz and 285 MHz by the CMNS scheme, with $\Delta f_{rep} =$ 47.46 MHz. A strong reduction of the phase noise of all modes is observed in the frequency range of 1 kHz to 1 MHz that was weakly affected by the PLL. At low Fourier frequencies below ~1 kHz, the phase noise of all lines coincides with the level achieved with the PLL and RF injection scheme alone. This results from the residual noise of the comb mode spacing, as shown in Section 3.1. A linewidth of 10 Hz, which mainly originates from the contribution of 50-Hz noise components, is obtained for the RF comb line n =3 with both master-follower and CMNS schemes. As the free-running linewidth of 1 MHz was reduced to only 700 kHz by the mutual stabilization between the two QCL combs, the CMNS brings a linewidth reduction of the RF comb lines by almost 5 orders of magnitude (from 700 kHz to 10 Hz).

The long-term frequency stability of the harmonic RF comb obtained with the CMNS was also assessed by recording the frequency of two lines $n = 1$ and $n = 7$ using a frequency counter and by processing the corresponding Allan deviation (see Fig. 3(c)). We observed sub-Hz frequency fluctuations at 1-s integration time for both lines. At a longer averaging time of 200 s, the frequency stability reaches a sub-mHz level for the line $n = 1$, while the other line achieves a value of 3 mHz. We believe that the increase of the Allan deviation observed for averaging times longer than 100 s is due to an improper referencing of the synthesizer used to frequency down-convert the line $n = 7$ to fit in the frequency range of the frequency counter. However, the achieved stability is fully suitable for the implementation of coherent averaging.

4. Proof-of-principle spectroscopic measurement with coherent averaging

We compared multiple measurements of the dual comb multi-heterodyne beat signal with and without stabilization. The former includes the full mutual lock between the two QCL combs and the CMNS scheme. We acquired time traces of the sample and reference signals at 2 GS/s and 16-bit resolution using the acquisition unit of the IRis-F1 spectrometer from IRsweep. The measurements are limited by the internal memory to 16-ms acquisition time, corresponding to 2^{25} samples per acquisition and channel. The conditions for coherent averaging requires the interferogram to be offset-free with the spacing between the modes well matched to the sampling rate [24,28]. These conditions also prevent spectral leakage in other systems based on Fourier-transform spectrometers [43]. They are fulfilled with the CMNS that leads to an offset-free RF comb and by setting Δf_{rep} so that 3 interferograms are contained in exactly 128 data samples, corresponding to $\Delta f_{rep} = 46.875$ MHz. However, the data acquisition unit was not referenced to the reference clock during the experiment, such that coherent averaging was limited to measurement times of approximately 100 µs, after which the sampling and the interferogram lose their coherence.

Optics EXPRESS

4.1. FFT spectra and coherent averaging

In Fig. 4(a)-(b), we show the fast Fourier transform (FFT) of the 16-ms time trace acquired without frequency stabilization and a zoom on a line. The typical linewidth is in the MHz range. The highest signal-to-noise ratio (SNR) in terms of power spectrum is approximately 50 dB. In Fig. 4(c), we show a fraction of the time trace containing 3 periods with different phase offsets (blue). We also draw the coherently-averaged signal (orange) with 2048 co-added slices of 128 samples. As the conditions for coherent averaging are not fulfilled, the coherently averaged signal averages to zero.

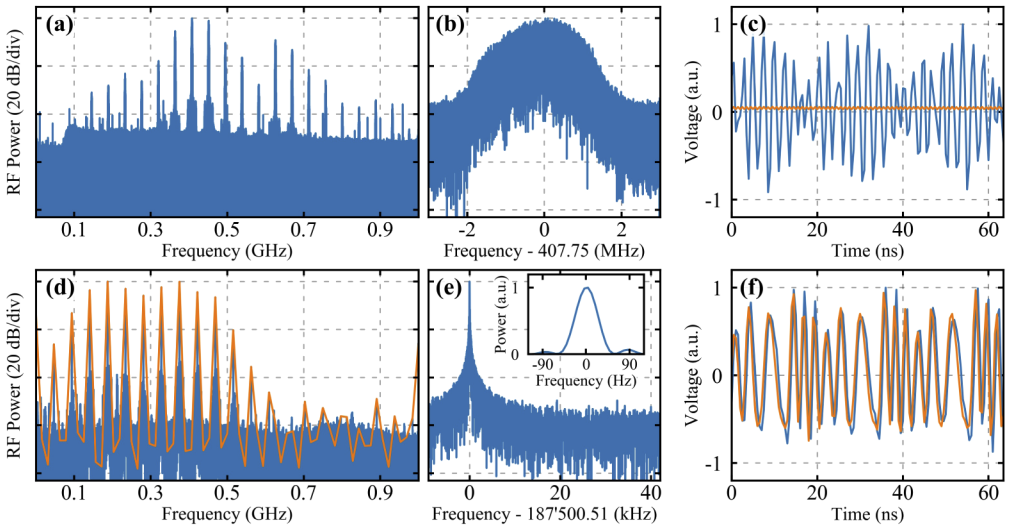

Fig. 4. (a) – (c) DCS results obtained without stabilization nor signal correction of the RF comb. (a) Spectrum obtained from the FFT of a 16-ms time trace. (b) Zoom of a line of panel (a). (c) Example time trace including approximatively 3 periods (blue). The signal averages out to zero when coherent averaging is performed (orange). (d) – (f) DCS results with master-follower and common-mode noise subtraction schemes. (d) Spectrum from a 0.13-ms time trace (blue) compared to that obtained with coherent averaging (orange). (e) Zoom of a comb line from a 16-ms time trace. The inset shows the linewidth of the comb line in linear scale, limited by the measurement time. The signal was zero-padded. (f) Example time trace (blue) compared to the coherent average of 2048 traces (0.13 ms). The phase slip led to losses of the high frequency components.

In Fig. 4(d), we show the FFT of a 130-µs time trace of the noise-compensated signal of the dual comb, and in orange, the spectrum obtained by coherently averaging the same time trace as 2048 slices of 128 samples. As the RF comb is harmonic and three interferograms are contained in 128 samples (Δf_{rep} = 46.875 MHz), every third bin of the spectrum lies on a comb line. We note that the SNR is much higher than in panel (a) even in a 10-times shorter measurement time as a result of the spectral stability. Panel (e) shows a closer view on the 4th line of the comb. Here the 16-ms signal was zero-padded to show the linewidth below 100 Hz (inset), as limited by the measurement time. The center frequency of 187,500,510 Hz is 510 Hz above the expected value of $4\cdot\Delta f_{rep}$ because of the mismatch between the internal clock of the acquisition unit and the reference clock used in the stabilization scheme. Figure 4(f) compares a single slice containing exactly 3 periods and the coherent average of 2048 slices. We notice a good correspondence, due to the high frequency stability of the RF comb. A difference is induced by the small phase slip occurring between the sampling frequency and Δf_{rep}, which can be seen as a small delay of the

Optics EXPRESS

average with respect to the single slice, or as a filter on the higher frequency components (fast changes), which are more sensitive to this mismatch.

4.2. Amplitude noise characterization

The fractional Allan deviation $\sigma_a(\tau)$ of the amplitude of different lines was computed for different integration times τ by slicing the time traces into segments of duration τ. For the CMNS, coherent averaging was applied (in the time domain) on each segment using slices of 128 samples and the amplitude of a line was obtained at specified bins of the Fourier transform of the coherently-averaged data, for each segment. A similar computation was performed in the free-running case. However, for a given segment and a given line, the amplitude was obtained by averaging the complex peak amplitudes obtained by a standard peak finder algorithm applied to the Fourier transform of all consecutive slices of 2048 samples contained in the segment. This method is labeled as SFT.

For comparison, computational phase corrections (PC) or phase and amplitude corrections (PAC) were implemented on the signals. For this purpose, the slices were co-averaged in the spectral domain, after the signal bins of the sample photodiode were divided by the phase factor or by the complex amplitude of the respective bin of the reference photodiode. This correction was applied similarly to the complex peak amplitude in the free-running case.

Moreover, to emulate an application where the signal is coherently-averaged in the data acquisition unit without software corrections at short timescales and corrected over longer timescales, we perform the following processing:

1. Segments of 66-µs duration of the signal (1024 slices of 128 samples) are coherently averaged without correction. Each segment is thus condensed into 128 samples by the coherent averaging.

2. We take the Fourier transform of each condensed 128-sample segment.

3. The Fourier transforms of the condensed segments are co-averaged by dividing the signal bins as with the above-mentioned PAC.

We label this method as HCA (hybrid coherent averaging). In practice, it would lead to a reduction by 3 orders of magnitude in the amount of data to be transferred, which could be further improved by referencing the clock of the acquisition unit.

The fractional Allan deviation of the amplitude of selected lines is shown in Fig. 5(a). CMNS with coherent averaging shows an improvement of the fractional amplitude noise as a function of the integration time τ as $\tau^{-1/2}$ (dot-dashed line). However, the phase slip resulting from the clock mismatch introduces a decrease in performance at integration times longer than 1 ms. Moreover, ground loops with noise peak frequencies of ~100 kHz add frequency noise which converts into amplitude noise in Fig. 5(a) at approximately 1-µs averaging times.

When PC or PAC is applied, the Allan deviation decreases as $\tau^{-1/2}$ up to the millisecond-range. These corrections effectively attenuate the effects of phase slips and ground loops. The corrections are also effective for HCA, where the compensation was done at time scales longer than the effect of the noise source. We note that the Allan deviation is computed from integration times of 66 µs for HCA, as it is the shortest time unit available for this processing method. In the free-running case [Fig. 5(b)], PAC corrections enable the same performance to be reached as with the other schemes. The limit in the ms-range is believed to arise from uncorrelated amplitude fluctuations in the signals from the two photodiodes, which originates from mechanical vibrations, e.g. induced by the fan of the photodetectors.

According to the Allan deviation at 8 ms, the short-term noise equivalent absorption (NEA) for the chosen line is estimated to $10^{-5}/\sqrt{\text{Hz}}$ for HCA using the CMNS and master-follower schemes, which is similar to the NEA reported in Ref. [38]. Free-running lasers with PAC yield

Optics EXPRESS

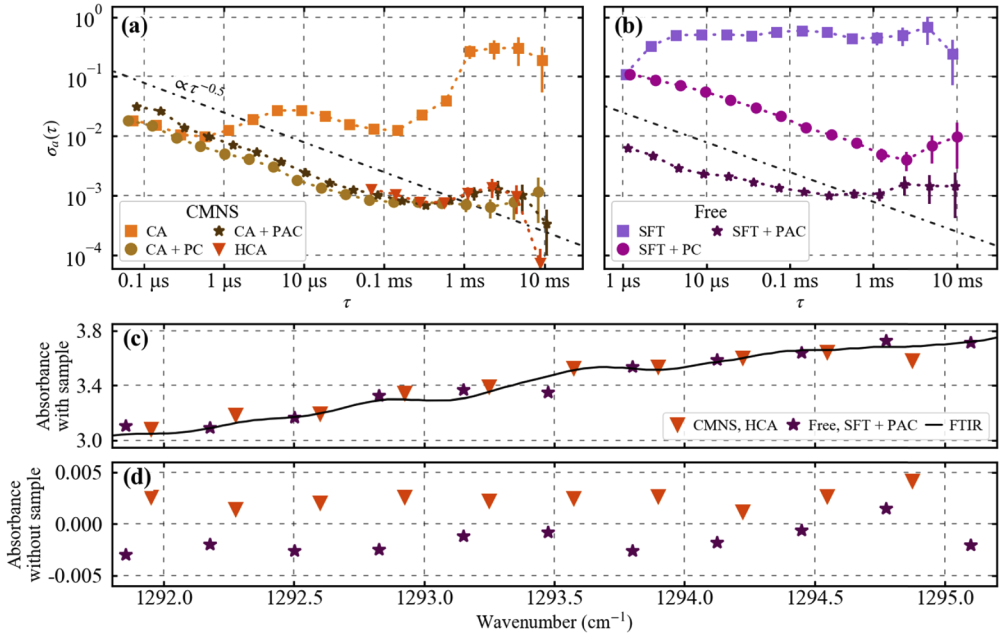

Fig. 5. Fractional amplitude Allan deviation σ_a and spectroscopic results. (a,b) Allan deviation of the amplitude of a selected line. Data points are offset horizontally for clarity. (a) Results with mutual stabilization and CMNS, with coherent averaging (CA), phase (and amplitude) correction (PC/PAC) and hybrid temporal and spectral averaging with correction (HCA). (b) Results without any stabilization of the QCL combs, where the amplitude of the RF comb lines is determined using a peak finder algorithm on Fourier transforms of slices (SFT). (c) Spectroscopic measurement of PP, compared to a spectrum measured with a standard FTIR. (d) Reference measurement with no sample showing accuracy better than 0.005, when the background measurement immediately follows the sample measurement.

approximately one order of magnitude higher NEA. These values are better than the value of $10^{-3}/\sqrt{\text{Hz}}$ reported in Ref. [20], where however the number of spectral components is one order of magnitude higher than in this study.

4.3. Spectroscopic measurements

A proof-of-principle spectroscopic measurement of polypropylene (PP) was made in order to demonstrate the suitability of the implemented schemes. A PP sheet with a thickness of 500 ± 5 µm was placed in the path of the combined QCL beams. The two fast photodiodes were used to provide sample and reference signals, respectively. The two photodiodes have different sensitivities, such that a background measurement was recorded in the absence of the sample to calibrate the respective photodiode signals.

The transmission of a given comb line was calculated as follows

$$T = \left| \frac{A_s B_r}{A_r B_s} \right|, \tag{1}$$

where A_i, B_i are the complex amplitudes of the line of the sample and background measurements, respectively. The subscripts denote the signal from the sample photodiode (s) or from the reference photodiode (r). The absorbance is calculated from the natural logarithm of T.

Results of the DCS experiment are shown in Fig. 5(c) for an acquisition time of 16 ms. We adjusted the frequency axis to match the absorption spectrum measured by DCS to an FTIR

Optics EXPRESS

reference measurement of the same sample, as no absolute optical frequency reference was available during the experiment to calibrate the optical frequency axis. The CMNS with HCA provides similar results as in free-running operation with PAC. They are consistent with the FTIR measurement within an error in the order of 0.05 in absorbance unit.

In the measurement without PP sample [Fig. 5(d)], two background measurements were performed immediately one after the other and compared using Eq. (1). The standard deviation of the absorbance is 0.0008 and 0.004 for the CMNS and free-running measurements respectively, consistent with the Allan deviation of approximately 0.001 in panels (a) and (b) of Fig. 5. However, a mean offset of 0.0024 and −0.0016, respectively, is observed from the theoretical value of 0 absorbance.

These results show that digital correction of phase noise and amplitude noise of the interferogram gives similar performance, whether the two QCLs are locked together or not. However, the mutual locking and the CMNS enable real time coherent averaging to be applied, which is a key condition to data reduction. Here, coherent averaging was successfully applied over up to 66 µs, which would lead to a data size reduction by 3 orders of magnitude if implemented in real-time. These results were limited by the phase slip of the data acquisition unit. Therefore, we expect that the amount of data can be further reduced by synchronizing the clocks to achieve longer real-time averaging.

5. Conclusion and outlook

We implemented a dual-QCL comb setup in a master-follower configuration. The offset frequency difference between the two combs was corrected by acting on the drive current of the follower QCL, while the repetition frequency difference was locked by electrical extraction from the master QCL, up-shifting, and injection in the follower QCL. We thus showed that two QCL combs can be mutually locked in both degrees of freedom simultaneously.

We observed that the actuation bandwidth for the stabilization of the offset frequency did not allow a significant reduction of the linewidth of the beat notes. Therefore, the frequency noise of the RF comb was further reduced using an all-RF common-mode noise subtraction scheme, which strongly reduced the common phase noise at Fourier frequencies between 1 kHz and 1 MHz.

These steps enabled fast and efficient sampling of the harmonic RF comb through coherent averaging using a minimum number of optical components for DCS. This allowed for reduced data handling and computational time in a proof-of-principle experiment, which promises real-time computation of the absorption spectra. It was shown that the amplitude noise of the comb lines is similar for both the frequency-stabilized and free-running systems, if computational corrections are implemented. The achieved short-term noise equivalent absorption is comparable with other studies such as reported in Ref. [38]. Therefore, the main motivation for the implemented mutual stabilization is to enable real-time data processing.

We expect that the multiple methods presented in this work will benefit QCL-based DCS by enabling more accurate measurements, owing to the increased possible averaging time. Also, the relative lock between the two QCLs is a steppingstone to a fully-referenced dual QCL comb system, where additionally, the accuracy of the frequency grid can be improved by the use of an optical reference in the mid-infrared.

The CMNS and the master-follower stabilization could be integrated in existing commercial systems, offering higher quality dual comb spectrometers. A next step is to apply the methods while scanning the offset frequency of the QCL combs to perform gapless spectroscopic measurements [4], where the challenge resides in the change of repetition rates during the scan.

Optics EXPRESS

Appendix

Common-mode noise subtraction scheme

An analog common-mode noise subtraction (CMNS) scheme is used to remove the offset frequency of the RF combs and the remaining common noise among their lines. The principle is to isolate one spectral line and to mix it with the entire RF comb to produce their frequency difference. The resulting RF comb is offset-free, i.e., it constitutes a harmonic comb, in which the common noise between all lines is removed. In practice, an RF mixer outputs both the sum and difference frequency of the input signals, resulting in two RF combs shifted from each other. SSB mixers, which produce only either the sum (SSB+) or the difference (SSB-) frequency of the two input signals, could be used to generate a single noise-compensated comb, but they are not available in the frequency range required here. Therefore, we first up-converted both the filtered single RF comb line by 2.5 GHz and the full RF comb by 2.5 GHz + $m \cdot \Delta f_{\mathrm{rep}}$ as schematized in Fig. 6, where m is an integer number and Δf_{rep} is the mode spacing of the RF comb. The single line is up-converted using an SSB+ mixer, while the comb is up-converted using a double balanced mixer followed by a high-pass filter to suppress the difference-frequency signal. The up-converted RF comb line and RF comb are then mixed, and the difference frequency component is selected using an appropriate filter. The resulting signal is a low-noise harmonic RF comb, as the frequency noise of the selected RF comb mode that was common to all comb lines has been subtracted.

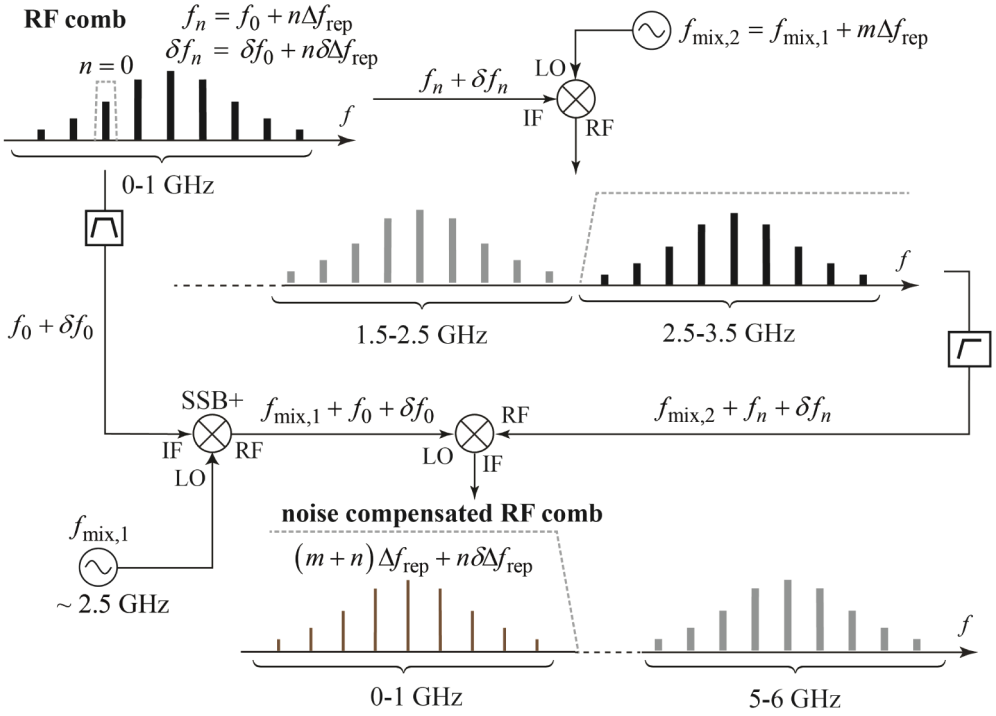

Fig. 6. Common-mode noise subtraction scheme. One line (indexed with $n = 0$) of the multi-heterodyne beat signal is filtered, and its frequency is shifted by $f_{\mathrm{mix},1}$ using an SSB mixer. The entire RF comb is also shifted by $f_{\mathrm{mix},1} + m \cdot \Delta f_{\mathrm{rep}}$ using a mixer and a high-pass filter. The two signals are mixed, such that their common noise is compensated, and the resulting low-noise RF comb is harmonic.

Funding. Swiss Space Office (MdP COSMICS); Schweizerischer Nationalfonds zur Förderung der Wissenschaftlichen

Optics EXPRESS

Forschung (2000020_178864, 20B2-1_176584); Horizon 2020 Framework Programme (871529).

Disclosures. The authors declare no conflicts of interest.

Data availability. Data underlying the results presented in this paper are available in Ref. [44].

References

1. I. Coddington, N. Newbury, and W. Swann, "Dual-comb spectroscopy," Optica **3**(4), 414–426 (2016).
2. A. Hugi, G. Villares, S. Blaser, H. C. Liu, and J. Faist, "Mid-infrared frequency comb based on a quantum cascade laser," Nature **492**(7428), 229–233 (2012).
3. G. Villares, A. Hugi, S. Blaser, and J. Faist, "Dual-comb spectroscopy based on quantum-cascade-laser frequency combs," Nat. Commun. **5**(1), 5192 (2014).
4. M. Gianella, A. Nataraj, B. Tuzson, P. Jouy, F. Kapsalidis, M. Beck, M. Mangold, A. Hugi, J. Faist, and L. Emmenegger, "High-resolution and gapless dual comb spectroscopy with current-tuned quantum cascade lasers," Opt. Express **28**(5), 6197–6208 (2020).
5. M. J. Norahan, R. Horvath, N. Woitzik, P. Jouy, F. Eigenmann, K. Gerwert, and C. Kötting, "Microsecond resolved infrared spectroscopy on non-repetitive protein reactions by applying caged-compounds and quantum cascade laser frequency combs," bioRxiv 2021.01.04.425172 (2021).
6. P. Fjodorow, P. Allmendinger, R. Horvath, J. Herzler, F. Eigenmann, M. Geiser, M. Fikri, and C. Schulz, "Monitoring formaldehyde in a shock tube with a fast dual-comb spectrometer operating in the spectral range of 1740–1790cm –1," Appl. Phys. B **126**(12), 193 (2020).
7. N. H. Pinkowski, S. J. Cassady, C. L. Strand, and R. K. Hanson, "Quantum-cascade-laser-based dual-comb thermometry and speciation at high temperatures," Meas. Sci. Technol. **32**(3), 035501 (2021).
8. N. H. Pinkowski, Y. Ding, C. L. Strand, R. K. Hanson, R. Horvath, and M. Geiser, "Dual-comb spectroscopy for high-temperature reaction kinetics," Meas. Sci. Technol. **31**(5), 055501 (2020).
9. G. Zhang, R. Horvath, D. Liu, M. Geiser, and A. Farooq, "QCL-Based Dual-Comb Spectrometer for Multi-Species Measurements at High Temperatures and High Pressures," Sensors **20**(12), 3602 (2020).
10. E. Lins, S. Read, B. Unni, S. M. Rosendahl, and I. J. Burgess, "Microsecond Resolved Infrared Spectroelectrochemistry Using Dual Frequency Comb IR Lasers," Anal. Chem. **92**(9), 6241–6244 (2020).
11. J. L. Klocke, M. Mangold, P. Allmendinger, A. Hugi, M. Geiser, P. Jouy, J. Faist, and T. Kottke, "Single-Shot Sub-microsecond Mid-infrared Spectroscopy on Protein Reactions with Quantum Cascade Laser Frequency Combs," Anal. Chem. **90**(17), 10494–10500 (2018).
12. U. Szczepaniak, S. H. Schneider, R. Horvath, J. Kozuch, and M. Geiser, "Vibrational Stark Spectroscopy of Fluorobenzene Using Quantum Cascade Laser Dual Frequency Combs," Appl. Spectrosc. **74**(3), 347–356 (2020).
13. T. J. Kippenberg, A. L. Gaeta, M. Lipson, and M. L. Gorodetsky, "Dissipative Kerr solitons in optical microresonators," Science **361**(6402), eaan8083 (2018).
14. S. Droste, G. Ycas, B. R. Washburn, I. Coddington, and N. R. Newbury, "Optical Frequency Comb Generation based on Erbium Fiber Lasers," Nanophotonics **5**(2), 196–213 (2016).
15. T. J. Kippenberg, R. Holzwarth, and S. A. Diddams, "Microresonator-Based Optical Frequency Combs," Science **332**(6029), 555–559 (2011).
16. J. Hillbrand, A. M. Andrews, H. Detz, G. Strasser, and B. Schwarz, "Coherent injection locking of quantum cascade laser frequency combs," Nat. Photonics **13**(2), 101–104 (2019).
17. F. Kapsalidis, B. Schneider, M. Singleton, M. Bertrand, E. Gini, M. Beck, and J. Faist, "Mid-infrared quantum cascade laser frequency combs with a microstrip-like line waveguide geometry," Appl. Phys. Lett. **118**(7), 071101 (2021).
18. M. R. St-Jean, M. I. Amanti, A. Bernard, A. Calvar, A. Bismuto, E. Gini, M. Beck, J. Faist, H. C. Liu, and C. Sirtori, "Injection locking of mid-infrared quantum cascade laser at 14 GHz, by direct microwave modulation," Laser Photonics Rev. **8**(3), 443–449 (2014).
19. P. Jouy, J. M. Wolf, Y. Bidaux, P. Allmendinger, M. Mangold, M. Beck, and J. Faist, "Dual comb operation of $\lambda \sim 8.2$ µm quantum cascade laser frequency comb with 1 W optical power," Appl. Phys. Lett. **111**(14), 141102 (2017).
20. J. Westberg, L. A. Sterczewski, F. Kapsalidis, Y. Bidaux, J. M. Wolf, M. Beck, J. Faist, and G. Wysocki, "Dual-comb spectroscopy using plasmon-enhanced-waveguide dispersion-compensated quantum cascade lasers," Opt. Lett. **43**(18), 4522–4525 (2018).
21. T. Ideguchi, A. Poisson, G. Guelachvili, N. Picqué, and T. W. Hänsch, "Adaptive real-time dual-comb spectroscopy," Nat. Commun. **5**(1), 3375 (2014).
22. O. Rompelman and H. H. Ros, "Coherent averaging technique: A tutorial review Part 1: Noise reduction and the equivalent filter," J. Biomed. Eng. **8**(1), 24–29 (1986).
23. I. Coddington, W. C. Swann, and N. R. Newbury, "Coherent dual-comb spectroscopy at high signal-to-noise ratio," Phys. Rev. A **82**(4), 043817 (2010).
24. E. Baumann, F. R. Giorgetta, W. C. Swann, A. M. Zolot, I. Coddington, and N. R. Newbury, "Spectroscopy of the methane ν 3 band with an accurate midinfrared coherent dual-comb spectrometer," Phys. Rev. A **84**(6), 062513 (2011).

Optics EXPRESS

25. A. M. Zolot, F. R. Giorgetta, E. Baumann, W. C. Swann, I. Coddington, and N. R. Newbury, "Broad-band frequency references in the near-infrared: Accurate dual comb spectroscopy of methane and acetylene," J. Quant. Spectrosc. Radiat. Transfer **118**, 26–39 (2013).
26. S. Okubo, K. Iwakuni, H. Inaba, K. Hosaka, A. Onae, H. Sasada, and F.-L. Hong, "Ultra-broadband dual-comb spectroscopy across 1.0–1.9 μm," Appl. Phys. Express **8**(8), 082402 (2015).
27. G.-W. Truong, E. M. Waxman, K. C. Cossel, E. Baumann, A. Klose, F. R. Giorgetta, W. C. Swann, N. R. Newbury, and I. Coddington, "Accurate frequency referencing for fieldable dual-comb spectroscopy," Opt. Express **24**(26), 30495–30504 (2016).
28. N. Hoghooghi, R. J. Wright, A. S. Makowiecki, W. C. Swann, E. M. Waxman, I. Coddington, and G. B. Rieker, "Broadband coherent cavity-enhanced dual-comb spectroscopy," Optica **6**(1), 28–33 (2019).
29. H. Guo, W. Weng, J. Liu, F. Yang, W. Hänsel, C. S. Brès, L. Thévenaz, R. Holzwarth, and T. J. Kippenberg, "Nanophotonic supercontinuum-based mid-infrared dual-comb spectroscopy," Optica **7**(9), 1181–1188 (2020).
30. J.-D. Deschênes, P. Giaccarri, and J. Genest, "Optical referencing technique with CW lasers as intermediate oscillators for continuous full delay range frequency comb interferometry," Opt. Express **18**(22), 23358–23370 (2010).
31. T. Ideguchi, A. Poisson, G. Guelachvili, T. W. Hänsch, and N. Picqué, "Adaptive dual-comb spectroscopy in the green region," Opt. Lett. **37**(23), 4847–4849 (2012).
32. J. Roy, J.-D. Deschênes, S. Potvin, and J. Genest, "Continuous real-time correction and averaging for frequency comb interferometry," Opt. Express **20**(20), 21932–21939 (2012).
33. D. Burghoff, Y. Yang, and Q. Hu, "Computational multiheterodyne spectroscopy," Sci. Adv. **2**(11), e1601227 (2016).
34. N. B. Hébert, J. Genest, J.-D. Deschênes, H. Bergeron, G. Y. Chen, C. Khurmi, and D. G. Lancaster, "Self-corrected chip-based dual-comb spectrometer," Opt. Express **25**(7), 8168–8179 (2017).
35. L. A. Sterczewski, J. Westberg, and G. Wysocki, "Computational coherent averaging for free-running dual-comb spectroscopy," Opt. Express **27**(17), 23875–23893 (2019).
36. Ł. A. Sterczewski, A. Przewłoka, W. Kaszub, and J. Sotor, "Computational Doppler-limited dual-comb spectroscopy with a free-running all-fiber laser," APL Photonics **4**(11), 116102 (2019).
37. M. Gianella, S. Vogel, K. Komagata, J. Hillbrand, F. Kapsalidis, B. Tuzson, A. Nataraj, A. Hugi, M. Mangold, P. Jouy, T. Südmeyer, S. Schilt, J. Faist, and L. Emmenegger, "Gapless high-resolution QCL dual-comb spectroscopy with real-time data processing for dynamic gas-phase measurements," Submitted to CLEO/Europe (2021).
38. J. Westberg, L. A. Sterczewski, and G. Wysocki, "Mid-infrared multiheterodyne spectroscopy with phase-locked quantum cascade lasers," Appl. Phys. Lett. **110**(14), 141108 (2017).
39. F. Cappelli, L. Consolino, G. Campo, I. Galli, D. Mazzotti, A. Campa, M. Siciliani de Cumis, P. Cancio Pastor, R. Eramo, M. Rösch, M. Beck, G. Scalari, J. Faist, P. De Natale, and S. Bartalini, "Retrieval of phase relation and emission profile of quantum cascade laser frequency combs," Nat. Photonics **13**(8), 562–568 (2019).
40. M. Piccardo, D. Kazakov, N. A. Rubin, P. Chevalier, Y. Wang, F. Xie, K. Lascola, A. Belyanin, and F. Capasso, "Time-dependent population inversion gratings in laser frequency combs," Optica **5**(4), 475–478 (2018).
41. G. Di Domenico, S. Schilt, and P. Thomann, "Simple approach to the relation between laser frequency noise and laser line shape," Appl. Opt. **49**(25), 4801–4807 (2010).
42. P. Brochard, S. Bilicki, A. Shehzad, S. Schilt, and T. Südmeyer, "Laser Linewidth Optimization in a Feedback Loop," in *2017 European Conference on Lasers and Electro-Optics and European Quantum Electronics Conference* (Optical Society of America, 2017), p. CH_4_3.
43. P. Maslowski, K. F. Lee, A. C. Johansson, A. Khodabakhsh, G. Kowzan, L. Rutkowski, A. A. Mills, C. Mohr, J. Jiang, M. E. Fermann, and A. Foltynowicz, "Surpassing the path-limited resolution of Fourier-transform spectrometry with frequency combs," Phys. Rev. A **93**(2), 021802 (2016).
44. K. Komagata, A. Shehzad, G. Terrasanta, P. Brochard, R. Matthey, M. Gianella, P. Jouy, F. Kapsalidis, M. Shahmohammadi, M. Beck, V. J. Wittwer, J. Faist, L. Emmenegger, T. Südmeyer, A. Hugi, and S. Schilt, "Data underlying the results presented in this paper are available at the EUDAT B2SHARE repository," b2share (2021)http://doi.org/10.23728/b2share.1ceecd3c598a420d8aba7254dae4ae2f